## Title

PARAMAGNETIC HYPERFINE STRUCTURE AND RELAXATION EFFECTS IN MOSSBAUER SPECTRA: Fe57 in FERRICHROME A



## Authors

Wickman, H.H.
Klein, M.P.
Shirley, D.A.

## Publication Date

1966-04-01

UCRL-16669

# University of California
# Ernest O. Lawrence Radiation Laboratory

PARAMAGNETIC HYPERFINE STRUCTURE AND RELAXATION EFFECTS IN MOSSBAUER SPECTRA: $Fe^{57}$ IN FERRICHROME A



Berkeley, California

## DISCLAIMER

Submitted to Physical Review

UCRL-16669

UNIVERSITY OF CALIFORNIA

Lawrence Radiation Laboratory
Berkeley, California

AEC Contract No. W-7405-eng-48

# PARAMAGNETIC HYPERFINE STRUCTURE AND RELAXATION EFFECTS IN MOSSBAUER SPECTRA: $Fe^{57}$ IN FERRICHROME A

H. H. Wickman, M. P. Klein, and D. A. Shirley

April 1966

# PARAMAGNETIC HYPERFINE STRUCTURE AND RELAXATION EFFECTS IN MÖSSBAUER SPECTRA: $Fe^{57}$ IN FERRICHROME A*

H. H. Wickman

Bell Telephone Laboratories, Inc.
Murray Hill, New Jersey

M. P. Klein and D. A. Shirley

Laboratory of Chemical Biodynamics,
Department of Chemistry and
Lawrence Radiation Laboratory
University of California
Berkeley, California

April 1966

## ABSTRACT

The Mössbauer effect of $Fe^{57}$ in the metalloprotein Ferrichrome A (FA) has been investigated at temperatures between 0.98 and 300°K; in some cases the absorber was placed in an external field of 18 kOe, oriented perpendicular to the propagation direction. The polycrystalline paramagnetic sample exhibited temperature-, field- and concentration-dependent magnetic hyperfine structure. At 0.98°K in zero field, a well resolved six-line spectrum was observed. As the temperature was raised, the pattern coalesced until at 300°K only a single broad non-Lorentzian line was visible. The effect of an applied field was, at all temperatures, to noticeably sharpen the hfs pattern; and at 77°K or below eight lines were easily resolved.

Changes of the spectra with temperature and field are attributed to electronic relaxation, and a simple model is used to calculate relaxation spectra. The model employs the modified Bloch equations as rate equations to describe fluctuations of an effective hyperfine field. The iron-iron separation

was increased by dilution of some of the samples in ethyl alcohol. As is well known from ESR work, spin-spin interactions decrease on dilution: a sharpening of the spectrum resulted. The importance of using solutions in studying Mössbauer spectra of biologically interesting $Fe^{3+}$ compounds is demonstrated.

Some of the consequences of paramagnetic hyperfine interactions for Mössbauer spectroscopy are discussed. Differences between the effective hyperfine field and the interaction $A\vec{I}\cdot\vec{S}$ are noted, as are certain analogies between Mössbauer and optical spectroscopy, under the $A\vec{I}\cdot\vec{S}$ interaction. From previous ESR work the electronic spin Hamiltonian for FA was found to be of the form $D[S_z^2-1/3\ S(S+1)] + E[S_x^2-S_y^2]$. Rather complex hyperfine spectra are predicted for $Fe^{3+}$ with this spin Hamiltonian, and representative spectra are illustrated. It is shown that these spectra, expected in the absence of spin-spin interaction, would be sufficient to determine the ratio, E/D, of the spin Hamiltonian parameters; this illustrates the complementary nature of ESR and Mössbauer spectra of the same system.

# I. INTRODUCTION

The application of many physical techniques to biological problems has been increasingly fruitful in recent years. Magnetic resonance methods have enjoyed wide application, while the Mössbauer effect (ME) has only recently begun to be employed in the study of biological systems.[1-3] A characteristic of magnetic resonance phenomena is their sensitivity to time-dependent processes affecting the fields responsible for the resonance conditions. Such effects are of course also present in ME experiments, although they have not been observed frequently.[4-6] In this paper we report the Mössbauer spectra of ferrichrome A (FA), which exhibits magnetic hyperfine structure in the paramagnetic state. Under a number of circumstances it is possible to observe the effects on these Mössbauer spectra of changes in the fluctuation rates among the electronic levels responsible for the magnetic hyperfine interaction.

Hyperfine interactions occur in three electronic crystal-field states of the $Fe^{3+}$ ion. These states, arising from the $Fe^{3+}$ ground level $^6S_{5/2}$, were characterized in previous ESR work. They are spaced by about one degree K.[7] It is convenient to lower the sample temperature so that only the lowest electronic doublet is appreciably populated, and is thereby mainly responsible for the observed hyperfine structure discussed in Sec. III. This spectrum is, as shown in Sec. IV, very sensitive to the crystal-field parameter ratio E/D. The parameters D and E could in principle be derived from a high resolution spectrum if dipolar or exchange interactions were absent.

The conditions under which the "hyperfine field" approximation may be applied to paramagnetic samples are also discussed in Sec. IV. One result is that for paramagnetic samples with long electronic relaxation times, crystal-field effects may often render inappropriate the interpretation of Mössbauer

spectra in terms of an effective magnetic field plus quadrupole interaction. These ideas are then applied in Sec. V to the low-temperature FA spectra.

Temperature-dependent features of the spectra are attributed to electronic relaxation, which is discussed in Sec. VI. A simple model, based on the modified Bloch equations, is used to calculate theoretical spectra that compare well with experiment and provide an estimate of the relaxation time.

## II. EXPERIMENTAL PROCEDURES

The structural formula of ferrichrome A appears in Fig. 1. It was first isolated and characterized by Neilands and Emory.[8] We are indebted to Prof. J. B. Neilands of the Biochemistry Department of the University of California at Berkeley for bringing these compounds to our attention. The isolation and purification of the materials were performed in Prof. Neilands' laboratory by the methods described in Ref. 9. Iron, enriched to 90% $Fe^{57}$, was incorporated into the molecules by Dr. R. A. J. Warren. The Mössbauer spectra were obtained with a conventional velocity-scanning spectrometer, in conjunction with a multichannel analyzer operating in the multiscalar mode. The room temperature source consisted of 10 millicuries of $Co^{57}$ diffused into metallic Pd. The width of the resonance observed with this source against an absorber of $Na_4Fe(CN)_6$ was 0.25 mm/sec.

The FA spectra were measured at several temperatures from 1.0°K to 300°K in zero field and in a transverse magnetic field of 18 kOe. A commercial helium dewar was modified to permit direct immersion of the sample into the liquid He bath for measurements in the temperature region from 4.2°K to 1.0°K.

This was accomplished by replacing the usual cylindrical He tail section with a rectangular pipe made from 3/4 × 3/8 inch waveguide. Holes were bored into the broad walls of the tubing and covered with pieces of 0.010 inch mylar which were bonded to the brass tubing by epoxy resin. The mylar sections were leak-tight against He(II) and provided a relatively transparent material for the 14-keV gamma rays. As the sample was completely contained in the liquid He its temperature was known with high accuracy from vapor pressure thermometry. We have found this procedure far more satisfactory than conduction cooling.

For temperatures intermediate between 4.2°K and 77°K we employed the technique of blowing cold He gas over the sample: A resistance thermometer, calibrated at several fixed temperatures, formed one arm of a Wheatstone bridge whose output, after suitable power amplification, was applied to a heater resistor immersed in the He storage dewar. The end of the He transfer tube within the storage dewar permitted only the He gas to be transferred to the sample dewar. Each desired operating temperature was selected by suitable choice of the bridge resistance. The system operated as a simple servomechanism, power being supplied to the heater resistor in just the correct amount to maintain the sensing resistor at the selected value. At temperatures above 10-12°K relatively modest quantities of liquid He were consumed; for lower temperatures the demand increased rapidly. The temperature accuracy above 4.2°K was ±2° while the temperature stability was somewhat better. A transverse magnetic field was provided by a 12" electromagnet.

The Mössbauer spectrometer was of the conventional linear velocity type employing a 400-channel analyzer. A tuning-fork oscillator operating at 5.0 Kc/s provided the "address advance" pulses for multiscaler operation. These pulses, scaled by a factor of four hundred, provided the pulses which initiated

each sweep of the multiscaler and set a flip-flop to one of its two states. Another pulse, scaled by 200 from the clock, set the flip-flop to its other state. The flip-flop output, a symmetric square wave, was then integrated to provide the reference triangular wave form for the velocity sweep and was accurately coherent with the address numbers. A Sanborn LV-Syn linear velocity transducer, mechanically coupled to the diaphragm of the loud-speaker drive motor provided, the input signal for the requisite feedback to assure highly linear velocity sweeps. While the latter feature is esthetically pleasing it was not required for reasons discussed below.

The velocity transducer was calibrated absolutely by an interferometric method as follows. A Michelson interferometer was formed with a fixed mirror rigidly attached to the beam splitter and the second mirror rigidly attached to the sample holder mounted on the loudspeaker. By careful adjustment of the angle between the two mirrors an interference pattern was formed and illuminated a photo detector. It is easy to show that the rate at which fringes are formed and lost, or the frequency at which fringes pass a fixed position, is equal to twice the velocity of the mirror divided by the wavelength of light. For the source of illumination we employed a small He:Ne gas laser. With this light source (the operating wavelength is 6328 Å), a velocity of one cm/sec produces a Doppler frequency of 31.6055 Kc/s. The photo detector was a Texas Instruments LS-600 phototransistor. The signals emanating from the phototransistor were suitably shaped and passed to the multiscaler. With the timing and velocity servomechanism operating normally, pulses from the interferometer were collected in the multiscaler memory for a measured period of time. The resultant waveform collected in the analyzer was a rectified triangular wave; the interferometer

cannot distinguish positive and negative velocities. The number of pulses in each channel, suitably corrected for analyzer dead-time, therefore corresponded to a particular easily calculable velocity.

For calibrating the electromagnetic velocity transducers it is convenient to convert their output voltage into a proportional pulse rate with a voltage-to-frequency converter and apply these pulses to the multichannel scaler. These voltage-to-frequency converters are highly linear, accurately calibrated in output pulse rate versus input voltage, and are stable; they may be designed to operate with either a zero output frequency or a biased output frequency for zero input voltage. Two runs of equal time, one of the interferometer and one with the v-f converter provide all the data necessary for calibrating the transducer; it is necessary only to determine the ratio of counts, on a channel-by-channel basis and apply the requisite conversion factors. A simple computer program plots the interferometer data versus the v-f data and computes the transducer calibration in (cm/sec)/volt. We have compared calibrations arrived at in this manner for at least six LVSyns with the more conventional method of employing the Mössbauer spectrum of metallic iron and find good agreement with the spacing between the outermost lines in the spectrum of Fe metal given by Hanna, et al.,[10] i.e., 1.061 cm/sec. Our value is 1.065 cm/sec.[11]

An experiment consists of the actual Mössbauer run, after which the data are punched out on paper tape, followed by a v-f run with the velocity spectrometer operating. Finally the velocity is set to zero and the zero-voltage v-f frequency is accumulated for exactly the same length of time as the v-f run. This last run serves to identify accurately the channel corresponding to zero velocity and as a normalizing run for the v-f run. A computer program also analyzes the velocity waveform, accumulated with the v-f

converter, fits the resulting curve with a polynomial of arbitrary degree and, using the calibration value for the velocity transducer, converts the channel numbers to velocities on an absolute scale.

We are indebted to Mr. Ronald Zane, who developed the spectrometer. Detailed technical descriptions of this apparatus and the interferometric calibration procedure will appear elsewhere.[12]

## III. EXPERIMENTAL RESULTS

The velocity spectra obtained with ferrichrome A in zero external field are shown in Fig. 2. Here positive velocity corresponds to absorber motion toward the source. At room temperature, a single broad line of half-width $\Gamma = 0.30 \pm 0.02$ cm/sec was observed. Although this width prevents observation of quadrupole splitting, an isomer shift of 0.02 cm/sec was determined; this shift is characteristic of $Fe^{3+}$ and is consistent with chemical evidence and electron spin resonance data. As the temperature was lowered, a continuous change in the spectra occurred, and at the lowest temperature the pattern consisted of six broad hyperfine lines.

To demonstrate that the samples were not magnetically ordered and did not contain sizable quantities of magnetic impurities we performed three independent experiments which showed the samples to be paramagnetic down at least to $1^{\circ}K$. Electron spin resonance experiments at 9 Gc were performed over the temperature range from $300^{\circ}K$ down to $1^{\circ}K$.[7] The spectra were at all temperatures characteristic of $Fe^{3+}$ and exhibited neither an unusual signal intensity nor any change of line positions which would be expected to occur upon magnetic ordering.

The bulk magnetic susceptibility of a crude sample of FA was measured as a function of temperature from 4.2°K down to 1.0°K and was found to obey a Curie's Law over this region. The mutual inductance bridge used for this measurement forms the magnetic thermometer for the nuclear alignment experiments performed in this laboratory and since it was a simple matter to do adiabatic demagnetization such an experiment was performed on a sample of Ferrichrome A. This experiment was modestly successful; the lowest magnetic temperature achieved was about 0.1°K. This implies that the FA is paramagnetic even well below 1°K.

Low-temperature experiments were also performed with an external field of 18 kOe transverse to the $\gamma$-ray direction. The results of the measurements are shown in Fig. 3. Because the sample was polycrystalline the actual absorption is an envelope of many resonances. The problem here is similar to the case of line shapes in the ESR of polycrystalline samples. We have, however, made the assumption that at 18 kOe the absorber is well polarized (this means that the nuclear-spin Hamiltonian is essentially diagonalized: see Sec. IV) and have fitted the data with sets of Lorentz curves. The procedure employed a program written by L. D. Wilson. The conclusions drawn from this approximation are suggestive rather than rigorous.

The qualitative features of the data show that at T ~ 1°K a very well resolved pattern is found. As the temperature is raised, two effects become pronounced. First, a noticeable broadening of the resolved lines occurs. Second, the resonant intensity in the central part of the spectrum increases markedly. We shall show in later sections that the former effect is characteristic of relaxation process, while the latter indicates the thermal population of the excited Kramers' doublets of the ion.

Finally, we show in Fig. 4 that the resolution of the low temperature spectrum may be sharpened considerably upon physical separation of the molecules by dilution in alcohol, and freezing of the solution into a glass. Dilution effects have also been observed in iron-doped corundum[4] and in certain glasses and inorganic compounds.[13,14] The effect here of course is to reduce spin-spin interaction and increase electronic relaxation times.

The line positions observed both in zero field and in the presence of an external magnetic field (where they are well-resolved) are given in Table I. While one would normally interpret this spectrum in terms of "hyperfine magnetic field" and quadrupole coupling parameters if the sample were in an ordered state, such a procedure is often inapplicable to a paramagnetic substance. We therefore discuss the Mössbauer effect in paramagnets in the next section before applying the results to the present experiments.

## IV. HYPERFINE FIELDS AND MÖSSBAUER SPECTRA

### A. The Spin Hamiltonian

The FA spectra reported above are quite similar, at the lowest temperatures, to the ordinary 6-line spectrum that $Fe^{57}$ exhibits in many ordered systems. In these systems a simplified nuclear spin Hamiltonian describes the level sequence in the presence of an "effective hyperfine field", $H_{eff}$. In a paramagnet, however, no simple analogue of $H_{eff}$ need exist and we must instead employ a more general Hamiltonian which also includes electron spin operators. It is appropriate to use the well-known "spin Hamiltonian" technique of ESR,[15] and we discuss below its application to Mössbauer spectroscopy.

A common spin Hamiltonian for a high spin $Fe^{+3}$ ion in low symmetry is

$$\mathcal{H}_{TOT} = \mathcal{H}_{Zeeman} + \mathcal{H}_{CF} + \mathcal{H}_{mhf} + \mathcal{H}_{Q} + \mathcal{H}_{N} + W \quad ,$$

where

$$\mathcal{H}_{Zeeman} = -\beta\vec{H}\cdot g\cdot\vec{S}$$

$$\mathcal{H}_{CF} = D(S_z^2-(1/3)\ S(S+1)) + E(S_x^2-S_y^2) \qquad (1)$$

$$\mathcal{H}_{mhf} = \vec{I}\cdot A\vec{S}$$

$$\mathcal{H}_{Q} = \vec{I}\cdot P\cdot\vec{I}$$

$$\mathcal{H}_{N} = -g_N\beta_N\vec{H}\cdot\vec{I}$$

The various operators represent the electronic Zeeman, crystal field, magnetic and electric hyperfine and nuclear Zeeman interactions. The constants involved here all have their usual meanings and S = 5/2 for $Fe^{3+}$. Another term not usually explicitly present in spin Hamiltonians is the constant W which denotes the shift in energy of a nuclear state and arises from its finite nuclear volume.[16]

In a Mössbauer absorption experiment there is, for a given chemical environment, a separate Hamiltonian, with (in general) different W, I, $g_N$, A, and P, for each nuclear level. The centroid of the absorption pattern is given by the isomer shift $\delta E$, which falls at

$$E = (W'_{ex}-W'_{g})_{source} - (W_{ex}-W_{g})_{absorber} \qquad (2)$$

where the prime notation allows for different chemical environments in source and absorber. We have written $\mathcal{H}$ to apply to $Fe^{3+}$ $^6S_{5/2}$ in a particular

crystalline field. The form of $\mathcal{H}$ is somewhat different for other ions or environments,[17] but the application to Mössbauer spectroscopy will be adequately illustrated by this form.

An eigenstate $\psi_i$ of $\mathcal{H}$ may be written in the $(2S+1)(2I+1)$-dimensional direct-product representation $|SMIm\rangle$ as

$$\psi_i = \sum_{M,m} a_i(Mm)|SMIm\rangle \quad . \tag{3}$$

The coefficients are of course functionally dependent on all the parameters in $\mathcal{H}$. The eigenstates $\psi_i$ can be rather strong admixtures of the basis vectors and it is worth noting that, for a $\gamma$-ray transition between nuclear states with spins I and I', there are $(2S+1)^2(2I+1)(2I'+1)$ possible components. The symmetry of the Hamiltonian and angular momentum selection rules will usually reduce this number substantially, but even for the FA case discussed below, as many as 16 separate lines, rather than the usual 6, are possible.

The transition selection rules are $\Delta M = 0$ and $\Delta m \leq k$, where $k$ is the rank of the tensor operator $\mathfrak{T}_k$ describing the nuclear transition. The transition matrix element is then

$$\langle \psi'_j | \mathfrak{T}^q_k | \psi_i \rangle = \sum_{\substack{M',M \\ m',m}} a^*(M,m)a(M',m')\langle I'm'kq|Im\rangle f_q(\theta) \times \langle I'\|\mathfrak{T}_k\|I\rangle \, \delta(M,M') \tag{4}$$

Application of this equation gives a complete description of the Mössbauer spectrum, which consists of components each with intensity $|\langle \psi'_j | \mathfrak{T}^q_k | \psi_i \rangle|^2$ at

energy $E'_j - E_i$, and with the usual polarization implied by $\mathcal{S}_k^q$. This is the static hyperfine pattern expected for long electronic relaxation times and in the absence of any fluctuating local fields.

## B. Magnetic Hyperfine Structure and Hyperfine Fields

The $\mathcal{H}_{mhf}$ term in $\mathcal{H}_{TOT}$ often gives rise to a hfs pattern that may be characterized by a "hyperfine magnetic field". This simply means that a new, nuclear, spin Hamiltonian of the form $\mathcal{H}' = g_N \beta_N \vec{H}_{hf} \cdot \vec{I}$ may be defined, where $\vec{H}_{hf}$ is a well-defined constant vector. $\mathcal{H}_{mhf}$ must, in these cases, be of the form $A\langle S_z \rangle I_z$. This is, of course, a quite restrictive form that need not hold in general; the problem of the actual form of $\mathcal{H}_{mhf}$ has been discussed in some detail.[15,17-20] However, it is useful to work through a few representative cases here, since no previous discussion has dealt in detail with the problem of paramagnetic hfs in Mössbauer spectra.

Since the hyperfine interaction is often much smaller than the crystal field interaction, we diagonalize first those terms in $\mathcal{H}_{TOT}$ depending on $\vec{S}$ but not $\vec{I}$: $\mathcal{H}_{CF} + \mathcal{H}_{Zeeman}$ neglecting $H_{hf}$. The problem is next restricted to a consideration of one of these (possibly degenerate) electronic energy levels at a time. For a non-degenerate electronic state with $\vec{S} = 0$ there is no hyperfine field. For degenerate levels an effective spin S' is defined such that $(2S'+1)$ is the degeneracy of the level.[19] It is then necessary to define a new operator within the manifold spanned by $\vec{S}'$ and I, in order to describe the effect of the hyperfine interaction. This is conventionally written as

$$\mathcal{H}(S',I) = A'_z S'_z I_z + A'_x S'_x I + A'_y S'_y I_y \qquad (5)$$

where the $A_i'$ depend on the crystal field parameters as well as on A in $\mathcal{H}_{mhf}$. (We shall assume that the actual electronic wave functions (represented by fictitious spin S') are spanned by a single $\vec{J}$ multiplet of the free-ion ground term; in this case J = 5/2.)

$\mathcal{H}$ may be effectively diagonalized in the $|S'M'Im\rangle$ representation by application of a polarizing field, $\vec{H}_p$, which may take the form of an externally applied magnetic field or, in a ferromagnetic lattice, the molecular (Weiss) field. If this field is taken along the z-axis, for example, large diagonal elements of the form

$$\langle S'M'Im|g_z'\beta H_p S_z'|S'M'Im\rangle = \sum_M |a_i(SM)|^2 g_J \beta M H_p \qquad (6)$$

result (here $g_J$ is the Landé g factor associated with S = J). In addition there is the direct interaction of the nucleus with $H_p$: i.e., $g_N\beta_N H_p I_z$. In paramagnets the latter term is overshadowed by the electron-nuclear hyperfine interaction which in turn, however, generally satisfies the relation $g_z'\beta H_p \gg A_x, A_y, A_z$. The resulting level spacing leads to the definition of an internal hyperfine field. In the high field limit and in the absence of mixing of crystal-field states, there are 2S'+1 groups of 2I+1 states each (if the Zeeman energy is large compared to the crystal-field energy, there are 2J+1 such groups, and the discussion that follows is applicable with only notational changes). The groups are separated by the electronic Zeeman energy $g_z'\beta H_p$ and may be considered separately. Within each group the 2I+1 nuclear substates are ordered and labeled by $I_z$ and are equally spaced by

$$\Delta E = A_z'\langle S_z'\rangle + g_N\beta_N H_p \quad . \qquad (7)$$

This spacing is formally equivalent to the interaction of the nuclear moment with an effective magnetic field of magnitude

$$H_{eff} = H_p + A_z \langle S'_z \rangle / g_N \beta_N \equiv H_p + H_{hf} \quad . \tag{8}$$

We have considered only the magnitude of the effective field and a different value would in general have been obtained had $H_p$ been directed along the x or y axes. In our simple case the net field at the nucleus is collinear with $H_p$. However it is easily shown that for a general orientation of $H_p$ with respect to the crystalline axes the nuclear quantization direction often differs from that of $H_p$.[20] The Mössbauer effect offers a particularly direct method of demonstrating this effect although no such experiments have been reported.

We now treat systematically the various possibilities for zero-field hfs arising from $\mathcal{H}(S',I)$. It is useful to rewrite the operator in the form (dropping the prime notation)

$$\mathcal{H}(S,I) = A_z S_z I_z + \frac{A_x + A_y}{4} [S_+ I_- + S_- I_+] + \frac{A_x - A_y}{4} [S_+ I_+ + S_- I_-] \quad . \tag{9}$$

There are four significantly different cases:

Case 1. Uniaxial Symmetry, $A_z \gg A_x = A_y \cong 0$ .

This case often occurs in the rare earths and the iron group. It appears in crystal fields with "axial" symmetry ($V_L^M = 0$ for $M \neq 0$ in the rare earths, or $D \neq 0$, $E = 0$ in Eq. (1)). Equation (9) leads to a set of $2I+1$ equally spaced doublets with eigenfunctions $|\pm M, \pm m\rangle$, and the Mössbauer spectrum is similar to a hyperfine field spectrum.[21] For $Fe^{57}$ this case was observed in

In the common case $S = 1/2$ and for dipole transitions the selection rule $\Delta F = 0, \pm 1$ applies. For $Fe^{57}$ with $I_e = 3/2$ and $I_g = 1/2$, a three-line spectrum is expected at energies of $3/4\ A_e - 1/4\ A_g$, $3/4\ A_g - 5/4\ A_e$, and $-5/4\ A_e + 1/4\ A_g$, with relative intensities 5:1:2. This is a simple example of an asymmetric hfs spectrum arising from an isotropic effective hfs interaction. The "hyperfine field" in this case (defined by application of a polarizing field, as above) is independent of the direction of polarizing field and has the magnitude $AS/g_N\beta_N$. It is interesting that the total distance between the outside lines for the case of $Fe^{57}$ is $2|A_e|+|A_g|$, which is larger than the splitting expected in a large external field: $3/2|A_e|+1/2|A_g|$. If $E_i$ and $N_i$ denote the energy and intensity of the $i^{th}$ component, we may determine the isomer shift from the sum rule

$$\delta E = \Sigma E_i N_i \tag{11}$$

The traceless interaction terms $A\vec{I}\cdot\vec{S}$ do not shift this centroid, as may easily be verified by direct substitution for the three components considered here.

Case 3: Axial Symmetry, $A_z \gg A_x = A_y$.

This is a very common case for rare earths in crystal fields with trigonal symmetry. We may write

$$\mathcal{H}(S,I) = AS_zI_z + \frac{A_x}{2}[S_+I_- + S_-I_+]. \tag{12}$$

For small $A_x$, the second term may be treated as a perturbation, introducing matrix elements of the form $\langle M\pm1, m\mp1|\mathcal{H}|Mm\rangle$ into Case 1 above. For $S = 1/2$

and half-integer nuclear spin, the $(4I+2)$-dimensional representation, diagonal for Case I, may be factored into 2 diagonal elements (for $|\pm 1/2, \pm I\rangle$) plus $2I$ $2 \times 2$-blocks. The doublet $|\pm 1/2, \mp 1/2\rangle$ is split (linearly in $A_x$) by $A_x(I+1/2)$, while the remaining doublets $|\pm 1/2, \mp m\rangle$ and $|\pm 1/2, \mp(m-1)\rangle$ originally spaced equally on either side of $|\pm 1/2, \mp 1/2\rangle$ are repelled (quadratically in $A_x$) by $(A_x^2/4A_z)\,[I(I+1) - m(m-1)]/(m-1/2)$ from their original positions. These pairs of doublets are spaced unsymmetrically with respect to the total hfs multiplet and do not include the $|\pm 1/2, \pm I\rangle$ doublet, which is unaffected (Fig. 5).

An asymmetric spectrum reflects this asymmetric level structure as shown in Fig. 6. In every case the $|\pm 1/2, \pm I_g\rangle$ to $|\pm 1/2, \pm I_e\rangle$ transition will be unchanged from Case B, while its partners will be shifted, and, if either nuclear spin is 1/2, unsplit. In $Fe^{57}$, for example, one of the intense outer lines is split, while the other is unaffected. The largest splitting, $|A_{x,g}|+2|A_{x,e}|$ occurs in the $\Delta m = 0$ transition connecting the outer components of the two $|\pm 1/2, \mp 1/2\rangle$ states. In low resolution the ten-line pattern could easily be mistaken for a six- or seven-line pattern, and the asymmetry mistaken for a quadrupole interaction.

Case 4: $A_z \gg A_x > A_y$

This situation will often occur in the iron group. $\mathcal{H}(S',I)$ is given by Eq. (9); the last term introduces matrix elements of the form $\langle \pm 1/2, m \pm 1 | \mathcal{H} | \mp 1/2, m\rangle$. The doublet $|\pm 1/2, \pm 1/2\rangle$ is most strongly affected, being split by $1/2(A_x - A_y)(I+1/2)$. By analogy to Case 3 those pairs of doublets $|\pm 1/2, \pm m\rangle$, $|\pm 1/2, \pm(m-1)\rangle$ that are symmetrically disposed about $|\pm 1/2, \pm 1/2\rangle$ are repelled by

$$\frac{(A_x - A_y)^2}{16A_z} \; \frac{I(I+1) - m(m-1)}{m-1/2}$$

from their original positions. For $Fe^{57}$ there will be 16 components. All the original lines are split, and the two original inner lines are each split into two doublets. This case is also illustrated in Figs. 5 and 6. In Table II the shifts in energy of the various lines are set out.

## V. ANALYSIS OF DATA

### A. Zero-Field Spectra

To analyze the data of Figs. 2-4 we apply the above arguments explicitly to the Hamiltonian $\mathcal{H}_{TOT}$ defined in the previous section. Truncation of $\mathcal{H}_{TOT}$ to

$$\mathcal{H}_{CF} = D[S_z^2-(1/3)\ S(S+1)] + E(S_x^2-S_y^2) \qquad (13)$$

leads to three Kramers' doublets and, when $\mathcal{H}_{mhf}$ is allowed to perturb each of them separately, to three sets of hyperfine tensors. The three hf tensors depend on the ratio $\lambda = E/D$ and within a doublet we have $A_x:A_y:A_z = g_x:g_y:g_z$ where the $g_i$ were the spectroscopic splitting factors for the doublet. The latter were given as functions of $\lambda$ in Ref. 7. In Fig. 7 the variation of the hyperfine tensors with the parameter $\lambda$ are shown. In Fig. 8 are shown the hfs spectra expected from each of the doublets for selected values of $\lambda$.

It is clear from Fig. 7 that some values of $\lambda$ exist for which all four cases discussed in Sec. II.B above are possible. Doublet 2 gives the isotropic Case 2 for $\lambda = 1/3$ and the uniaxial Case 1 for $\lambda = 0$ (for which $|\pm\rangle = |\pm 3/2\rangle$).

For $0 < \lambda < 1/3$, doublet 2 follows Case 4, but $A_x \cong A_y$ and it approaches Case 3. Doublet 3 is uniaxial (Case 1) at $\lambda = 0$. With increasing $\lambda$ it goes through Case 3 to Case 4. At $\lambda = 1/3$, doublets 3 and 1 are equivalent within a change of axes. As $\lambda$ decreases from 1/3 to 0 in doublet 1, $A_x$ and $A_z$ diverge and the spectrum is recognizable as Case 4. Finally, for $\lambda = 0$, doublet 1 shows a spectrum very different from that expected in the effective hyperfine field approximation.

From this discussion it is clear that a detailed study of the Mössbauer hyperfine structure spectrum in the long relaxation time limit and for cases in which dipolar effects are negligible (see below) can completely determine $A_x$, $A_y$, $A_z$, and the ratio $E/D$. This high sensitivity to crystal-field parameters provides incentive to study iron-containing biological compounds at the lowest temperatures.

It is immediately obvious on comparison of Figs. 2 and 8 that the experimental spectra do not resemble the calculated spectra for any value of $\lambda$. There are nowhere in the data more than 8 resolvable lines and careful analysis shows that a maximum of six lines may be associated with any one of the three electronic doublets. Four distinct effects are responsible for the differences: (1) dipolar interactions, (2) varied thermal populations of different levels, (3) quadrupole coupling, and (4) relaxation effects.

Spin-spin interactions can easily diagonalize the $A\vec{I}\cdot\vec{S}$ interaction in FA to within the limits of experimental sensitivity, reducing the 16-line spectrum expected in the absence of spin-spin effects to a six-line spectrum. This is particularly easy to see in the case of FA, because the ground doublet has $g_y \gg g_x$, $g_z$ and, thus approximates a dipole with a reasonable well-defined

magnetic field. This situation may be contrasted with the case of the ground doublet with $g_x = g_y = 3g_z$ occurring in $Fe^{3+}:Al_2O_3$. Here there is "magnetization in a plane", and no simple dipole field approximation is possible.

There are several Fe atoms within 10 Å of each resonant atom, and the spin-spin interaction with any one of these is of the order of $\sim\mu^2/r^3 = 2 \times 10^{-18}$ erg. The off-diagonal elements of $A\vec{S}\cdot\vec{I}$ in the lowest doublet are of the order of ASI, $\sim 2 \times 10^{-19}$ ergs, and one can easily show by perturbation theory that they affect the positions of the hfs components by a fractional shift of order $\sim(ASI)^2(\mu^2/r^3)^{-2} = 10^{-2}$. A complete numerical analysis of the dipolar interaction problem would be very tedious, but it is evident that this estimate is an upper limit on the expected shift. The large number of statistical spin arrangements to be associated with the neighboring Fe atoms that can provide significant contributions to the spin-spin interaction, together with the observed linewidth, preclude further study of this problem in undiluted samples. Evidently dilution to an average spin-spin separation of at least 20 Å is required to allow effective observation of the more complex (and more informative) sixteen-line spectra. If this dilution is achieved by using solutions, molarities of 0.5 M or less are thus required.

The effects of dilution are illustrated in Fig. 4, where we have plotted the spectrum of a 0.1 M (frozen) solution of FA in ethanol. It is clear that dilution offers a simple technique for sharpening Mössbauer lines. In a sample consisting of iron-organic complexes, dilution by solution in an appropriate solvent and freezing of the solution into a glass is particularly advantageous because the immediate environment of the iron atom is unlikely to be significantly altered.

In Ref. 7 it was reported that the energy spacing between adjacent Stark doublets derived from the $^6S_{5/2}$ manifold was of the order of magnitude of k(5°K), from the qualitative observation that relative intensities in the spin-resonance spectrum changed appreciably in the liquid helium temperature range 1-4°K. A more accurate estimate was not feasible from these data, but from the zero-field spectra shown in Fig. 2 we estimate that the two lowest doublets are separated by k(1-1.5)°K.

In view of the above discussion it would appear at first sight unlikely that even the lowest temperature zero-field spectra (Fig. 2) could be fitted by a simple Hamiltonian of the form

$$\mathcal{H} = g_e \beta_N H_{hf} I_y + P[I_y^2 - (1/3)\, I(I+1)] \qquad (14)$$

for the excited state and a similar expression (with P = 0) for the ground state. We have tested this Hamiltonian by forcing a fit, by allowing $H_{hf}$ to vary between the ground and excited states. We find the isomer shift $\delta E$ = +0.038 cm/sec, P = 0.037 cm/sec, $H_{hf}$ (ground state) = 520 kgauss, $H_{hf}$ (excited state) = 545 kgauss. Of the 5% discrepancy in $H_{hf}$, only 1% can be attributed to experimental error. Thus we conclude that the above form of $\mathcal{H}$ is inadequate.

Any attempt at more detailed analysis of the zero-field spectra would be pointless in view of the large experimental linewidths and the multiplicity of parameters involved. We shall, however, extract three parameters from these spectra. The isomer shift, $\delta E$ = +0.038 cm/sec, is relatively independent of the finer details of the spectrum, and is probably valid. The total splitting,

1.729 cm/sec, between the outer lines is relatively insensitive to $\lambda = E/D$ and almost completely insensitive to $P$ and $\eta$ in the range of interest for FA. In Ref. 7 we found $\lambda = 0.25 \pm 0.04$. The ratio (total splitting between centers of gravity of outer doublets)/(total splitting arising from $H_{hf}$ in a diagonal representation in which $\langle S_z \rangle = 5/2$) varies from 0.925 for $\lambda = 0.21$ to 0.958 for $\lambda = 0.29$. We thus may derive a $H_{hf}$ for the diagonal representation of $|H_{hf}| = 571 \pm 10$ kgauss from the observed splitting and this range of $\lambda$.

## B. hfs in an External Field

The application of an external magnetic field leads in general to a much more complicated picture for the hyperfine interactions. However, because $g_L \beta H \gg D,E$ at fields of the order of 20 kOe, the $|SM\rangle$ states are effectively quantized along the external field direction. Thus, although polycrystalline samples were employed, at high fields the electronic Zeeman pattern is expected to be independent of the orientation of a particular crystallite relative to the field direction. The hfs will show an effective field pattern for each appreciably populated level, with hyperfine fields proportional to $\langle S \rangle$ for the particular state.

The overall Zeeman splitting is ~10°K and with a separation of the two lower levels of ~2°K, we expect, at 1°K, a superposition of only two effective field patterns. One corresponds to a field of $(5/2)(220) \cong 550$ kOe, the other to $(3/2)(220) \cong 330$ kOe; where we use the conversion factor of 220, for the hyperfine field per spin expectation value, typical of paramagnetic high spin $Fe^{3+}$.[23] For each electronic level the relative intensities of the hfs are

3:4:1:1:4:3. This approximation assumes pure $|M,m\rangle$ states and any observed deviations are measures of the validity of the approximation.

In Fig. 3 there are eight lines at the lowest temperature; the six intense lines arise from the ground electronic substate $|M = -5/2\rangle$, and the two least intense lines come from the next electronic substate, $|M = -3/2\rangle$. The latter two lines correspond to the pair with relative intensity 4 noted above, as illustrated in Fig. 9. The effective fields (uncorrected for the applied field) for the two hfs patterns are 535 and 329 kOe; their ratio is 0.62 compared with 0.60 expected for the high field Zeeman limit. A forced fit of these 18 kG data to an effective field Hamiltonian yields very good agreement between the field determined from the ground state alone, 532 kG, and that determined from the excited state alone, 536 kG. This is expected if the above discussion of the origins of the hyperfine pattern is correct. If the (weighted) effective field of 535 kG is taken as negative and is corrected for the applied field of 18 kgauss (at 1.0°K the polycrystalline sample is polarized sufficiently that the two fields can be taken as collinear), we find $H_{hf}$ = -553 kgauss, in excellent agreement with the value -550 kG[23] for the $Fe^{3+}$ ion obtained from double resonance.

Analysis of the low temperature data of Fig. 2 showed that an appreciable quadrupole splitting is present in FA. However, we find that this effect decreases from P = 0.037 cm/sec to 0.009 cm/sec on addition of an external field of 18 kOe (Fig. 3). In the polycrystalline absorber in zero field, we had $\vec{H}_{eff} \| \vec{P}$; however, with the polarizing field present $\vec{H}_{eff}$ is now parallel to $\vec{H}_p$. The relative orientation of $\vec{P}$ and $\vec{H}_{eff}$ becomes random provided $\vec{P}$ arises from the environment of the ion rather than from its spin. This

effects an averaging of $P(3\cos^2\theta-1)$ over $0 \leq \theta \leq \pi$; this average vanishes and the apparent quadrupole coupling from this source will decrease, although some broadening remains. This broadening is evidently offset in large measure by the sharpening of the lines due to an increase of the relaxation times in the presence of the field. The observed behavior thus establishes that at least the major part of the EFG does indeed arise from the environment of the $Fe^{3+}$ ion, rather than being associated with the spin.

## VI. RELAXATION EFFECTS

Recently a number of observations of paramagnetic hyperfine structure have been reported.[4-6,24,25] In general these results are typified by a nuclear resonance pattern whose shape depends rather critically on the rate of electronic relaxation processes that are responsible for the magnetic hyperfine fields at the nucleus.[26] Here we describe a simple approximation that is sufficient to describe several important features of such spectra. Since our first calculations of relaxation spectra[27] a number of discussions have appeared which treat the problem from various viewpoints.[28-31] Of course the results of these theories agree well in limiting cases with the simple approach sketched below.

From the nuclear standpoint, relaxation effects arise from (random) fluctuations of the internal fields which are assumed to be of electronic origin. In FA the electric fields arise from extraionic charge distributions that are not expected to fluctuate in a manner directly affecting the nucleus. For this reason we assume that the fluctuating fields at the nucleus are solely

of magnetic origin. The simplest case is a nucleus exposed to a hyperfine magnetic field $\vec{H} = (0,0\pm H)$ directed along the z-axis, but which at a given instant of time may have one of two possible polarities. As discussed in some detail above, this requires a specific form of hyperfine interaction. For simplicity we consider only an isolated electronic doublet with effective spin 1/2. As a general criterion for the hyperfine field $\vec{H}$, we noted that it is sufficient to have the relations among the principal values of the effective hyperfine tensor: $A_z \gg A_x \cong A_y \cong 0$. For example, the $|M = \pm 5/2\rangle$ and $|M = \pm 3/2\rangle$ states in axial symmetry (Fig. 7, $\lambda = 0$) satisfy this criterion. Of immediate relevance here, however, is that the ground Kramers doublet in FA also satisfies the criterion as shown in Fig. 7 for $\lambda \approx 0.25$.

For such cases one identifies the operator $(A/g_N\beta_N)S_z$ with an effective field as above. It follows that the $|+5/2\rangle$ state, for example, implies a field with polarity opposite to that of the $|-5/2\rangle$ state. Thus, the forbidden transitions from the $|+5/2\rangle$ to $|-5/2\rangle$ levels would result in a reversal of the field at the nucleus. In the following, we consider a crystal field doublet $|\pm\rangle$ which in general need not be an angular momentum eigenstate, but has $A_z \gg A_x, A_y$; it is obvious that

$$\langle +|S_z|+\rangle = -\langle -|S_z|-\rangle \quad ; \tag{15}$$

thus the remarks on field polarity remain valid. However, transitions between the electronic states are no longer forbidden, and it is within the context of such transitions that the resultant change in Mössbauer resonance spectra may be discussed. The nuclear energy levels associated with the $|+\rangle$ and $|-\rangle$ levels

are given by the level scheme of Fig. 10. The effect of the electronic (relaxation) transition $|+\rangle \rightarrow |-\rangle$ is to change the "low energy" nuclear transition $\omega_i^+$ to the high energy transition $\omega_i^-$. Notice that $\Delta m_I = 0$ during the electronic process. It is not really necessary to specify the relaxation mechanism in detail, since we are only considering the effect at the nucleus of an electronic transition. It is sufficient to characterize the process $|+\rangle \longleftrightarrow |-\rangle$ by a characteristic time $\tau_e$ which will be the mean "spin-flip" lifetime, of the level $|+\rangle$ or $|-\rangle$. This could occur via dipolar relaxation and the parameter $\tau_e^{-1}$ would vary as $|\langle +|S_+|-\rangle|^2$. Since the Mössbauer effect yields a measurement of the energy levels associated with the scalar interaction $AI\cdot S \approx \vec{\mu}\cdot\vec{H}_{eff}$, it is clear that either of the static level schemes will produce the same resonance pattern.[21,27] It is also clear that if the transitions $\omega_i^+ \longleftrightarrow \omega_i^-$ occur many times within the nuclear lifetime, no net internal field will be found since the time average $\langle S_z \rangle$ then vanishes. These two limiting cases correspond respectively to a resolved six-line hyperfine pattern, and to a single unsplit line. The rough criteria for resolved hyperfine structure are simply $\tau_e$, $\tau_N \geq \omega_L^{-1}$, where $\omega_L$ and $\tau_N$ are respectively the Larmor precession frequency and mean life of the first excited state. Such criteria of course follow directly from the uncertainty principle.

It is interesting now to note that the Mössbauer conditions described above share the essential features of an already existing model describing the effects of proton exchange in nuclear magnetic resonance. The phenomenological model for proton exchange employs the modified Bloch equations,[32,33] whose solutions have been given.[34] In the following we show how these solutions may be applied to the Mössbauer case and easily interpreted in terms of the relaxation process discussed above. In the simple case we have considered, pairs of the

12 allowed transitions shown in Fig. 10 are related and become interchanged in energy after a spin-flip, i.e., a relaxation event. The related pairs are those with equal intensity, and if we focus our attention on a single nuclear transition the change in field polarity may be viewed as a random frequency modulation of the resonance transition. Once a pair of frequencies are available for a given Mössbauer transition, it is necessary to determine the Mössbauer spectrum for this transition as a function of the relaxation rate between them.

The response $\vec{G}$ of the system is required such that the resonance absorption $I(\omega)$ is given by $I(\omega) = \mathrm{Re}\vec{G}$ or $\mathrm{Im}\vec{G}$. Since relaxation is occurring, $\vec{G}$ will have a time dependence and will depend on the number of frequencies available to a particular transition. In the simple two-frequency problem they are denoted by $\omega_A$ and $\omega_B$. What is needed is a set of rate equations for a system possessing two such resonant frequencies. For these we take the modified Bloch equations in the rotating frame,[34] with $\vec{G} \equiv \vec{G}_A + \vec{G}_B$ ,

$$\frac{dG_A}{dt} + \alpha_A G_A = -iI_A + \tau_B^{-1} G_B - \tau_A^{-1} G_A \qquad (16a)$$

$$\frac{dG_B}{dt} + \alpha_B G_B = -iI_B + \tau_A^{-1} G_A - \tau_B^{-1} G_B \ . \qquad (16b)$$

These are simple coupled differential equations with

$$\alpha_A = \Gamma_A - i(\omega_A - \omega) \qquad (17a)$$

$$\alpha_B = \Gamma_B - i(\omega_B - \omega) \qquad (17b)$$

expressing the fixed frequencies and natural line widths of the resonances at $\omega_A$ and $\omega_B$; we will assume $\Gamma_A$ and $\Gamma_B$ to be equal and denote this width by $\Gamma$. The quantities $I_A$ and $I_B$ in the NMR case are proportional to magnetization in the rotating frame times the rf magnetic field inducing NMR transitions, and to the relative probability of the frequencies $\omega_A$ and $\omega_B$. The analog for the Mössbauer case would be the electromagnetic multipole operator inducing the $\gamma$-ray transition, and of course the relative probability of two related frequencies, say $\omega_i^+$ and $\omega_i^-$. The intensity factor is therefore simply given by the square of the appropriate Clebsch-Gordan coefficient for the transitions $\omega_i^{\pm}$. We neglect any difference in populations over the hyperfine levels and in the absence of any external field, $\omega_i^+$ and $\omega_i^-$ are equally probable. This need not be true in general however, and the relative populations are commonly denoted $p_A$ and $p_B$. These correspond to the relative probabilities of the two possible field polarities. For our case $p_A$ and $p_B$ are taken equal, and $I_A$ and $I_B$ are equal to the relative intensity of the lines at $\omega_A$ and $\omega_B$, in the limit of slow relaxation. For example, if $\omega_A$ and $\omega_B$ correspond to $\omega_i^+$ and $\omega_i^-$, then $I_A = I_B = 3$, for a polycrystalline absorber. The parameter $\tau_B^{-1}$ gives the probability per unit time of a transition from $\omega_B$ to $\omega_A$. We could write $p_{BA} = \tau_B^{-1}$; similarly $p_{AB} = \tau_A^{-1}$. We require the steady state solutions where $\dot{G}_A = \dot{G}_B = 0$, and define the conventional parameters $\tau = (\tau_A\tau_B)/(\tau_A+\tau_B)$, $p_A = (\tau_A)/(\tau_A+\tau_B)$, and $p_B = 1 - p_A$. Taking $p_A = p_B$ is equivalent, in steady state, to $\tau_A = \tau_B$. The solutions to Eq. (16) are given by

$$I(\omega) = \mathrm{Im}(G) = \mathrm{Im}(G_A+G_B) = - I[(1+\tau\Gamma)\, P+QR]/(P^2+R^2) \qquad (18)$$

where

$$P = \tau\{\Gamma^2 - [\tfrac{1}{2}(\omega_A+\omega_B - \omega]^2 + \tfrac{1}{4}(\omega_A-\omega_B)^2\} + \Gamma \qquad (19a)$$

$$Q = \tau[\tfrac{1}{2}(\omega_A+\omega_B) - \omega - \tfrac{1}{2}(p_A-p_B)(\omega_A-\omega_B)] \qquad (19b)$$

$$R = [\tfrac{1}{2}(\omega_A+\omega_B) - \omega](1+2\tau\Gamma) + \tfrac{1}{2}(p_A-p_B)(\omega_A-\omega_B) \quad . \qquad (19c)$$

These solutions may now be immediately adapted to the effective-field problem. Notice that in fact there are six independent allowed Mössbauer transitions, and hence six pairs of related frequencies. In our simple example, $\omega_i^{\pm}$ and $\omega_{7-i}^{\pm}$ behave in the same manner, so it is sufficient to consider only $\omega_i^{\pm}$, i = 1, 2, 3. The unperturbed $\gamma$-ray energy may be set equal to zero and the frequencies $\omega_1^{\pm}$, $\omega_2^{\pm}$, and $\omega_3^{\pm}$ are obtained from Table I. The relative intensities of $\omega_1^{\pm}$, $\omega_2^{\pm}$, $\omega_3^{\pm}$ are 3:2:1. The total intensity is written as a sum of three sets of solutions to Eq. (16) for the three relative intensities just mentioned. The total intensity is

$$I_{TOT} = I_{TOT}(\tau,\omega) = \sum_{i=1}^{3} I_i(\tau,\omega_i^+,\omega_i^-,\omega) \qquad (20)$$

Spectra based on these solutions are given in Fig. 11, using a Hamiltonian of the form of Equation (14), with $H_{eff}$ = 550 kOe. The differential broadening of the pairs of related transitions is made obvious by plotting the components $I_1$, $I_2$, and $I_3$. This is the origin of asymmetric broadening of quadrupole spectra and has been discussed separately.[28,35] Further unusual effects arising from different population factors, $p_A$ and $p_B$, will be given elsewhere.

Comparison of Fig. 11 and Fig. 2 establishes an effective relaxation time of $\tau = 0.1$ μsec for the ground doublet. This is a zero-field estimate of the relaxation rate and the data in Fig. 3 shows clearly that a magnetic field leads to a splitting of the electronic levels and to a reduction in the overlap of the hyperfine levels relative to the zero field situation. For each temperature relaxation in a field of ~10 kOe tends to be slower than in zero field. Studies in a similar system (N benzoyl-ferrioxamine B) as a function of external field have shown explicitly this decrease in relaxation rate as a function of external field. Details of these effects will be published separately.

Returning to Fig. 2, it is evident that as the temperature is raised, higher doublets are populated and a diffuse contribution to the spectrum causes the hyperfine spectrum to "sag". On subtracting the computed relaxation spectrum for the lowest doublet from the observed data, we find a diffuse broad resonance similar to the 300°K spectrum. The origin of this resonance is the middle doublet, which should have a much shorter effective relaxation time than the upper or lower doublet since dipolar relaxation will probably dominate and $|\langle +|S_+|-\rangle|$ is appreciable here. On the other hand the upper doublet satisfies the effective field criteria (Fig. 7), and would contribute an effective field pattern similar to the ground doublet, but it is not populated at temperatures for which relaxation times are long.

Finally we note that the comments above concerning the relaxation model may be slightly generalized in a simple way. We associated with each electronic level a single hyperfine field and for a doublet there are two absorption frequencies. Upon application of a magnetic field the crystal field levels are split and each level can yield a different hyperfine field. If all three

Kramers' doublets are split then one has six frequencies to consider for each Mössbauer transition, and a more general set of coupled equations are required; these are[32]

$$G_n + \alpha_n G_n = -iI_n + \sum_k (P_{kn} G_n - P_{nk} G_k) \quad . \tag{21}$$

A steady-state form of these equations may be written as a matrix and solutions obtained by computer techniques.

In conclusion, we point out that the explicit calculation of the transition probability for general cases does not appear an easy task at this time. For FA, with the restriction to the ground doublet, the matrix elements of $\langle + | S+ | - \rangle$ can be calculated, and they give a simple interpretation for the $|+\rangle \longleftrightarrow |-\rangle$ type of relaxation.[27] This, however, is an extremely simple case. When considering relaxation in the presence of a field, the composition of the electronic wave function may change and the $P_{ij}$ now depend on the field value. Hyperfine mixing will also occur, so that finally $P_{ij}$ is functionally dependent on a least 5 independent variables.

REFERENCES

1. U. Gonser and R. W. Grant, Biophys. Journ. 5, 823 (1965).
2. A. J. Bearden, T. H. Moss, W. S. Caughey, and C. A. Beaudveau, Proc. Nat'l. Acad. Sej. 6, 1246 (1965).
3. D. C. Blomstrom, E. Knight, Jr., W. D. Phillips, and J. F. Weiher, Proc. Nat'l. Acad. Sci. 51, 1085 (1964).
4. G. K. Wertheim and J. P. Remeika, Phys. Letters 10, 14 (1964).
5. H. Dobler, G. Petrich, S. Hufner, P. Kienle, W. Wiedemann, and H. Eicher, Phys. Letters 10, 319 (1964).
6. S. Ofer, B. Khurgin, M. Rakavy, and I. Nowik, Phys. Letters 11, 205 (1964).
7. H. H. Wickman, M. P. Klein, and D. A. Shirley, J. Chem. Phys. 42, 2113 (1965).
8. T. Emory and J. B. Neilands, J. Am. Chem. Soc. 83, 1626 (1961).
9. T. Emory and J. B. Neilands, J. Am. Chem. Soc. 82, 3658 (1960).
10. R. S. Preston, S. S. Hanna, and J. Heberle, Phys. Rev. 128, 2207 (1962).
11. We are indebted to Ronald Zane, Lawrence Radiation Laboratory, for determination of this value.
12. Ronald Zane, Lawrence Radiation Laboratory, private communication.
13. C. R. Kurkgian and D. N. E. Buchanan, Phys. Chem. Glasses 5, 63 (1964).
14. J. W. G. Wignall (private communication to HHW, 1965).
15. A. Abragam and M. H. L. Pryce, Proc. Roy. Soc. A205, 135 (1951).
16. O. C. Kistner and A. W. Sunyar, Phys. Rev. Letters 4, 412 (1960).
17. R. J. Elliott and K. W. H. Stevens, Proc. Roy. Soc. A218, 553 (1953).
18. B. Bleaney and K. W. H. Stevens, Rept. Progr. Phys. 16, 108 (1953).
19. K. D. Bowers and J. Owen, Rept. Progr. Phys. 18, 304 (1955).

20. B. Bleaney, Phil. Mag. [7] 42, 441 (1951).

21. H. H. Wickman and I. Nowik, Phys. Rev., to be published.

22. H. Kopfermann, "Nuclear Moments", (Academic Press, New York, 1958). There are many analogies between Mössbauer and atomic spectroscopy, too obvious to belabor here.

23. P. R. Locher and S. Geschwind, Phys. Rev. 139, A991 (1965).

24. F. E. Obenshain, L. D. Roberts, C. F. Coleman, D. W. Forester, and J. O. Thomson, Phys. Rev. Letters 14, 365 (1965).

25. M. Clauser, E. Kankeleit, and R. L. Mössbauer, Bull. Am. Phys. Soc. 10, 1202 (1965).

26. A. M. Afanas'ev and Yu. Kagan, Soviet Phys. JETP 18, 1139 (1964).

27. H. H. Wickman, Ph.D. Thesis, University of California, Berkeley (1964), UCRL-11538; H. H. Wickman, M. P. Klein, and D. A. Shirley, Bull. Am. Phys. Soc. 10, 576 (1965).

28. M. Blume, Phys. Rev. Letters 14, 96 (1965).

29. F. van der Wonde and A. J. Dekker, Phys. Status Solidi 9, 775 (1965).

30. H. Wegener, Z. Physik 186, 498 (1965).

31. E. Bradford and W. Marshall, private communication.

32. H. S. Gutowsky, D. W. McCall, and C. P. Slichter, J. Chem. Phys. 21, 279 (1953).

33. H. M. McConnell, J. Chem. Phys. 28, 430 (1958).

34. J. A. Pople, W. G. Schneider, and H. J. Bernstein, "High-Resolution Nuclear Magnetic Resonance," (McGraw-Hill Book Co., Inc., New York, 1959) Chap. 10.

35. H. H. Wickman and A. M. Trozollo, Phys. Rev. Letters 15, 156 (1965).

Table I. Line positions for FA at 1°K.[a]

| Line no. | 1 | 2 | 2' | 3 | 4 | 5' | 5 | 6 |
|---|---|---|---|---|---|---|---|---|
| Field | | | | | | | | |
| zero | -7.97 | -4.85 | --- | -1.18 | 1.33 | --- | 4.97 | 9.32 |
| | -92.4 | -56.3 | | -13.7 | 15.4 | | 57.7 | 108.3 |
| 18 kgauss | -8.17 | -4.72 | -3.54 | -1.07 | 1.60 | 2.66 | 5.21 | 9.04 |
| | -94.8 | -54.8 | -41.1 | -12.4 | 18.6 | 30.9 | 66.2 | 105.0 |

[a]Doppler velocities in mm/sec. Accuracy is ±0.05 mm/sec; also given below are the positions in Mc/sec.

Table II. $Fe^{57}$ transition energies under the Hamiltonian $\mathcal{H} = A_z S_z I_z + A_x S_x I_x + A_y S_y I_y$, with S = 1/2.

| Line number N | $E_N$, for $A_x=A_y=0$[a] | Energies for $A_z \gg A_x=A_y$[b] | Energies for $A_z \gg A_x > A_y$[c,d] |
|---|---|---|---|
| 1 | $-\frac{1}{4}A_z' - \frac{3}{4}A_z$ | $E_1 - \frac{1}{2}A_x' - \frac{3}{4}A_x^2/A_z$<br>$E_1 + \frac{1}{2}A_x^2 - \frac{3}{4}A_x^2/A_z$ | $E_1 - P$<br>$E_1 + P$ |
| 2 | $-\frac{1}{4}A_z' - \frac{1}{4}A_z$ | $E_2 - A_x - \frac{1}{2}A_x'$<br>$E_2 + A_x + \frac{1}{2}A_x'$ | $E_2 - M - P$<br>$E_2 + M + P$ |
| 3 | $-\frac{1}{4}A_z' + \frac{1}{4}A_z$ | $E_3 - A_x'/2 + \frac{3}{4}A_x^2/A_z$<br>$E_3 + A_x'/2 + \frac{3}{4}A_x^2/A_z$ | $E_3 - N - P$<br>$E_3 - N + P$<br>$E_3 + N - P$<br>$E_3 + N + P$ |
| 4 | $\frac{1}{4}A_z' - \frac{1}{4}A_z$ | $E_4 - A_x$<br>$E_4 + A_x$ | $E_4 - M - Q$<br>$E_4 - M + Q$<br>$E_4 + M - Q$<br>$E_4 + M + Q$ |
| 5 | $\frac{1}{4}A_z' + \frac{1}{4}A_z$ | $E_5 + \frac{3}{4}A_x^2/A_z$ | $E_5 - N - Q$<br>$E_5 + N + Q$ |
| 6 | $\frac{1}{4}A_z' + \frac{3}{4}A_z$ | $E_6$ | $E_6 - Q$<br>$E_6 + Q$ |

[a] All $A_i$, $A_i'$ above denote absolute values. Primes refer to ground state. For arranging according to energy, A was taken positive (negative) in the excited (ground) state.

[b] To terms of order $A_x^2/A_z$.

[c] To terms of order $A_x, A_y$.

[d] $M \equiv \frac{1}{2}(A_x+A_y)$, $N \equiv \frac{1}{2}(A_x-A_y)$, $P \equiv \frac{1}{4}(A_x'+A_y')$, $Q \equiv \frac{1}{4}(A_x'-A_y')$.

FIGURE CAPTIONS

Fig. 1. The structural formula of ferrichrome A. The six oxygens nearest iron atom actually form a distorted octahedron.

Fig. 2. Mössbauer spectra of a FA absorber, taken against a source of $Co^{57}$ in Pd, at various temperatures between 0.98 and 300°K. At the highest temperature the hfs pattern collapses into a single, non-Lorentzian line. This lineshape is explained theoretically in Sec. VI: it can be obtained from the Bloch equations. The thick absorber produces a deviation of the intensity ratios from 3:2:1:1:2:3 at lowest temperature.

Fig. 3. Mössbauer spectra as in Fig. 2, but with an external magnetic field of 18 kG applied perpendicular to $\gamma$-ray beam. Electronic relaxation rate is decreased, as expected, in this field. Curves represent least-squares fits for eight Lorentzians of equal width. Theoretical explanation of these curves is given in Sec. V.B, and Fig. 9.

Fig. 4. Spectrum of a magnetically dilute sample of FA, consisting of 0.1 M frozen ethanol solution, at 4.2°K. Dipole-dipole ($T_2$) relaxation is strikingly slowed by dilution, as expected (compare middle curve of Fig. 2), but immediate environment of iron atom within FA molecule is unaffected. Note quadrupole effects on spacing of four outer lines, as in Fig. 2. Nearby spins in solution still tend to diagonalize $\mathcal{H}_{mhf}$, but lower intensity of line 2 (near -0.5 cm/sec) relative to line 5 may be first indication of the emergence of sixteen-line zero-field spectrum illustrated in Figs. 5 and 6 for the case $A_y \gg A_z, A_x$. Linewidths are ~0.05 cm/sec.

Fig. 5. Level structure and $\gamma$-ray transitions (relative intensities given across top) for a Kramers doublet in $^{57}Fe^{3+}$ under the Hamiltonian $A_z S_z I_z + A_x S_x I_x + A_y S_y I_y$.

Fig. 6. Expected Mössbauer spectra for levels shown in Fig. 5. The lower spectra should be present in very dilute paramagnets.

Fig. 7. Principle values of the effective hyperfine tensors for the three Kramers doublets formed from $^6S_{5/2}$ under the Hamiltonian $D[S_z^2-(1/3)S(S+1)] + E(S_x^2-S_y^2) + A\vec{S}\cdot\vec{I}$, plotted against $\lambda = E/D$. Note that all of the cases discussed in Sec. IV.B are found here.

Fig. 8. Exact calculated curves of Mössbauer absorption spectra expected for $Fe^{57}$ in the three Kramers doublets produced from $^6S_{5/2}$ by $\mathcal{H} = D[S_z^2-(1/3)S(S+1)] + E(S_x^2-S_y^2) + A\vec{S}\cdot\vec{I}$, for various values of $\lambda = E/D$. Notation of labels is (value of $\lambda$), (number of doublet). See Fig. 7. Zero-velocity point and relative scale are shown on each spectrum. The scale used for these calculated spectra corresponds to a $H_{hf}$ for $\langle S\rangle = 5/2$ of 355 kG, rather than the value 550 kG usually found in $Fe^{3+}$. All the limiting cases shown in Figs. 5 and 6 and discussed in Sec. V.B are found here.

Fig. 9. Origin of spectra shown in Fig. 3. Fig. 9(a): At left is shown the removal of sixfold electronic degeneracy in $^6S_{5/2}$ by polarizing field $H_p$. Simultaneous diagonalization of $AS\cdot I$ gives $H_{hf} = 220\ \langle S_z\rangle$ kG in each electronic substate. Corresponding transverse $Fe^{57}$ spectra are shown at right. Fig. 9(b): Mössbauer absorption spectra expected when all $S_z$ levels are equally populated ($g\beta H_p \ll kT$) and when lowest level is dominant ($g\beta H = kT$). These two spectra were obtained from those in Fig. 9(a) by appropriate weighting and using Lorentz lines. Agreement is excellent with top and bottom experimental spectra in Fig. 3, considering thick-absorber effects in latter.

Fig. 10. Effect of electron relaxation on hyperfine component in Mössbauer spectra of $Fe^{57}$. Consider the $(I,m_I = 1/2, -1/2)$ to $(I,m_I = 3/2, -3/2)$ component, to illustrate the effect of relaxation. For electron spin up (left), this is a low-energy transition, $\omega_1^+$ appearing (along with the component $\omega_6^-$) in "line 1) of the 6-line spectrum. Spin flip increases the transition energy, as the hyperfine field is now reversed, and component $\omega_1^+$ becomes $\omega_1^-$ (with the same nuclear quantum numbers), appearing now in line 6 of the six-line spectrum. Rapid relaxation causes the hyperfine field to average to zero, and the six lines merge into one.

Fig. 11. Relaxation spectra for the FA pattern, $H_{eff} = 550$ kOe. Transitions $\omega_{1,6}^{\pm}$ in Fig. 10 are represented by curves $I_1$, $\omega_{2,5}^{\pm}$ by curve $I_2$ and $\omega_{3,4}^{\pm}$ by curve $I_3$. The total Mössbauer pattern is the superposition of the three components which were drawn separately to emphasize the differential rate of collapse. Comparison with data gives an estimate of relaxation rate. Note that the three spectra for the three shortest relaxation times exhibit the asymmetric broadening of the doublet arising from quadrupole splitting of the excited state.

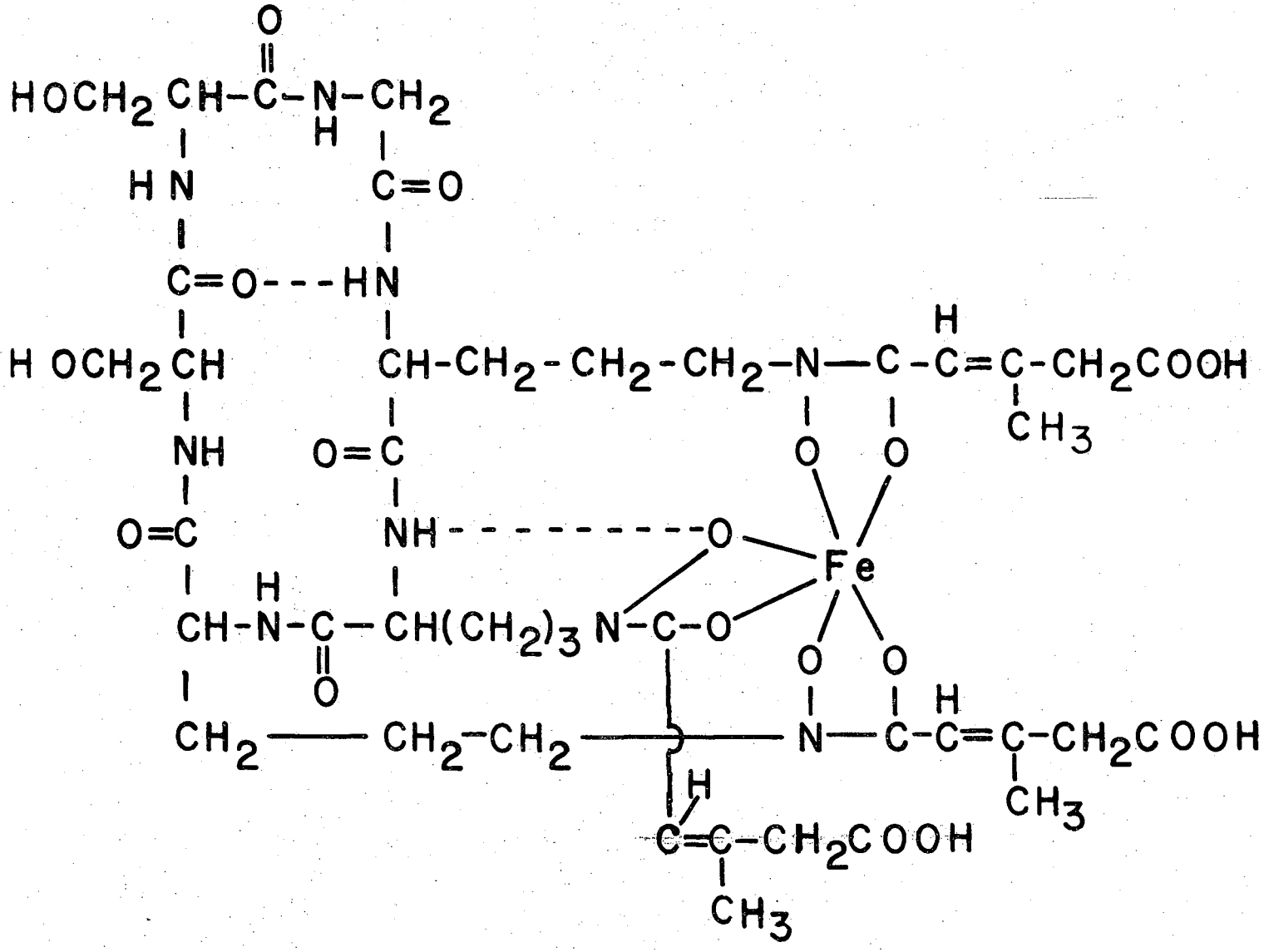
HOCH2 CH-C-N-CH2
O
H
HN
C=O
C=O---HN
H OCH2 CH
CH-CH2-CH2-CH2-N—C-C=C-CH2COOH
H
CH3
NH
O=C
O=C
O
O
NH
O
Fe
CH-N-C-CH(CH2)3 N-C-O
H
O
O
O
CH2 — CH2-CH2 — N—C-C=C-CH2COOH
H
CH3
C=C-CH2COOH
CH3

Fig. 1

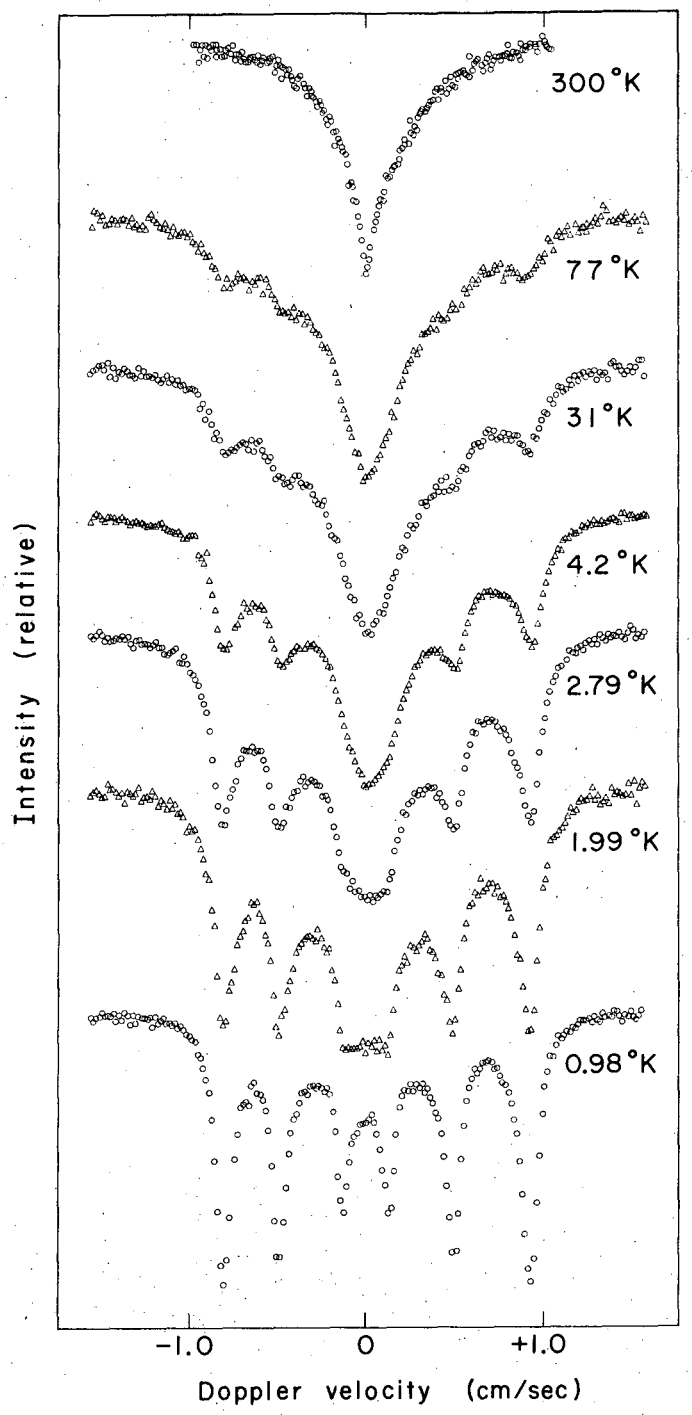
300 °K
77 °K
31 °K
4.2 °K
2.79 °K
1.99 °K
0.98 °K
Intensity (relative)
-1.0
0
+1.0
Doppler velocity (cm/sec)

Fig. 2

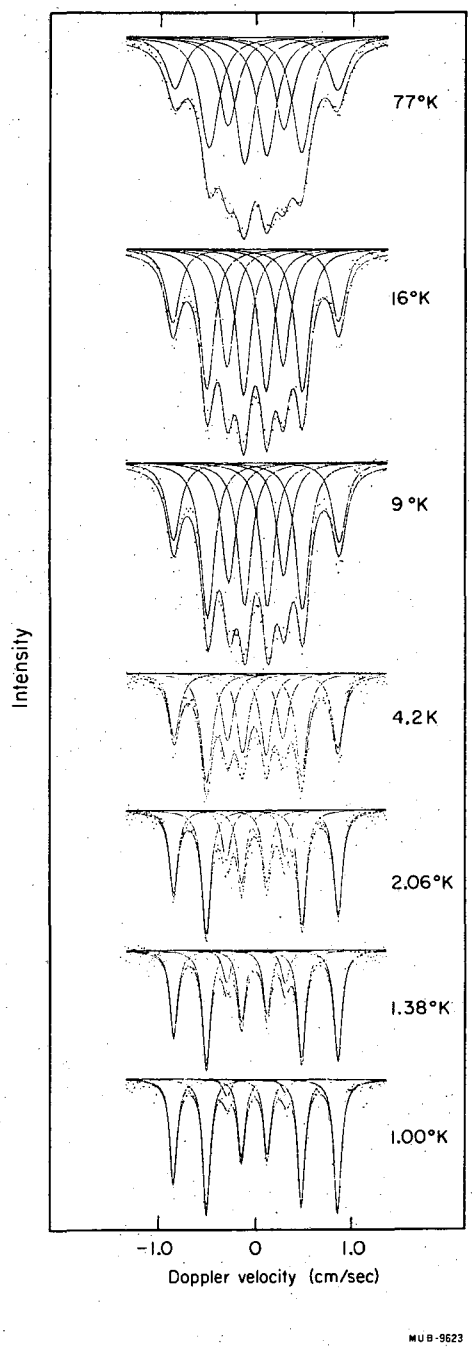
77°K
16°K
9 °K
4.2K
2.06°K
1.38°K
1.00°K
Intensity
-1.0
0
1.0
Doppler velocity (cm/sec)
MUB-9623

Fig. 3

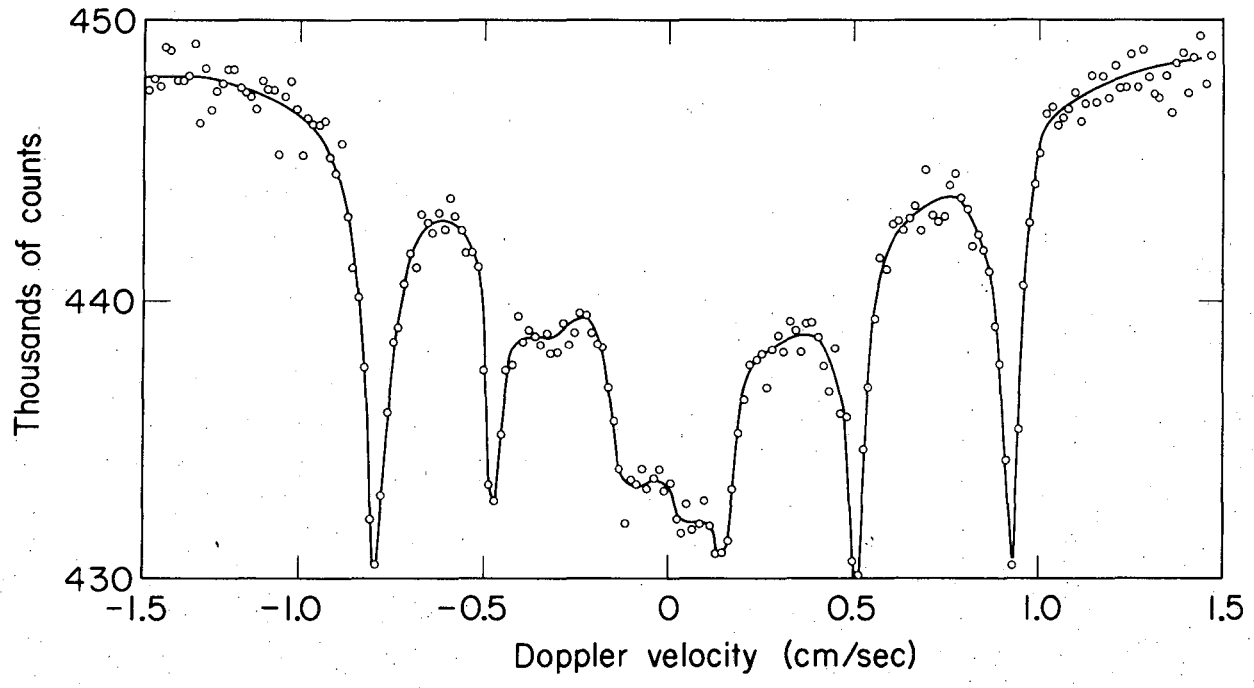
450
440
430
Thousands of counts
-1.5
-1.0
-0.5
0
0.5
1.0
1.5
Doppler velocity (cm/sec)
MUB-9555

Fig. 4

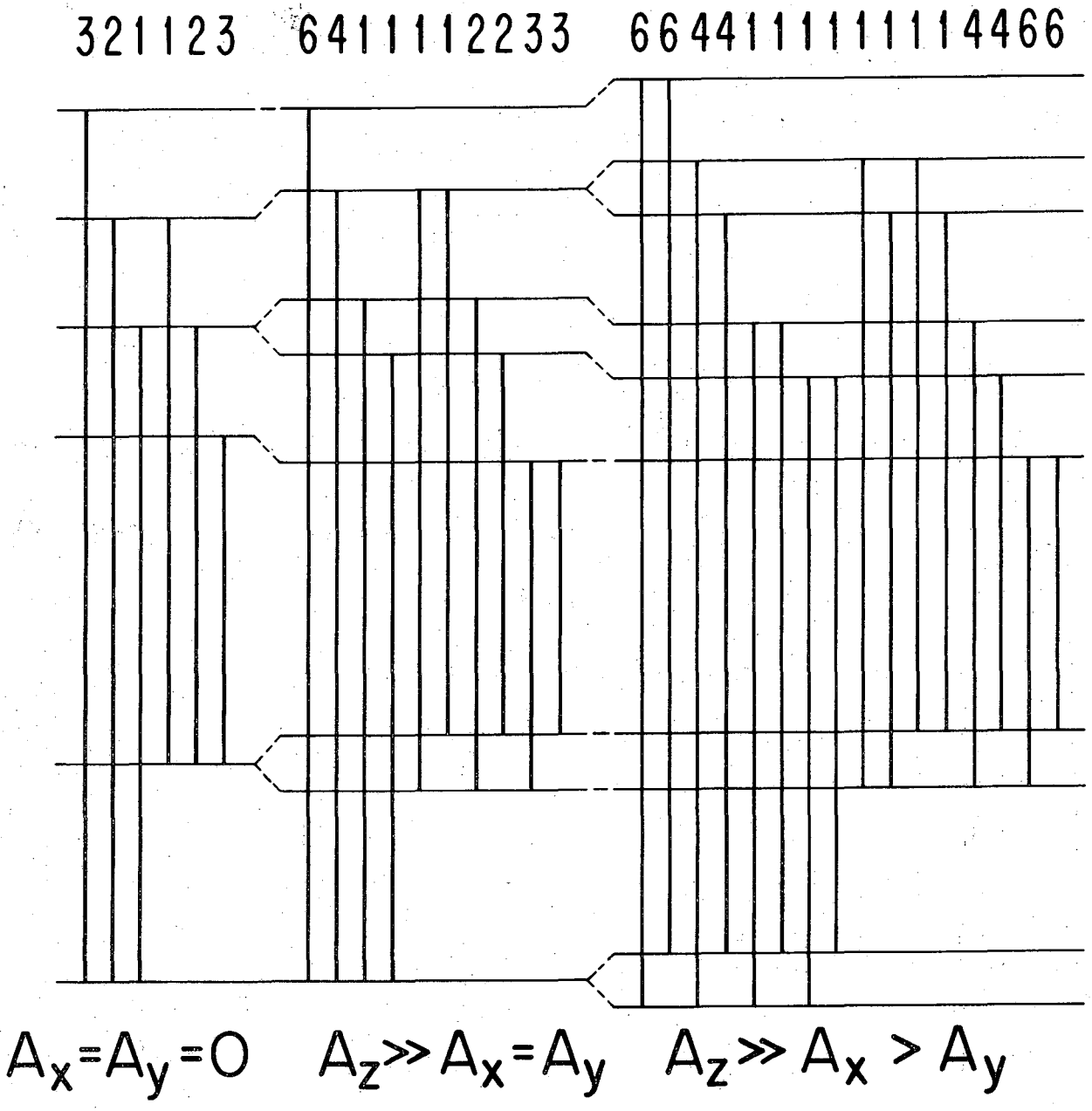
321123
6411112233
6644111111114466
$A_x=A_y=0$
$A_z \gg A_x=A_y$
$A_z \gg A_x > A_y$
MUB-9558

Fig. 5

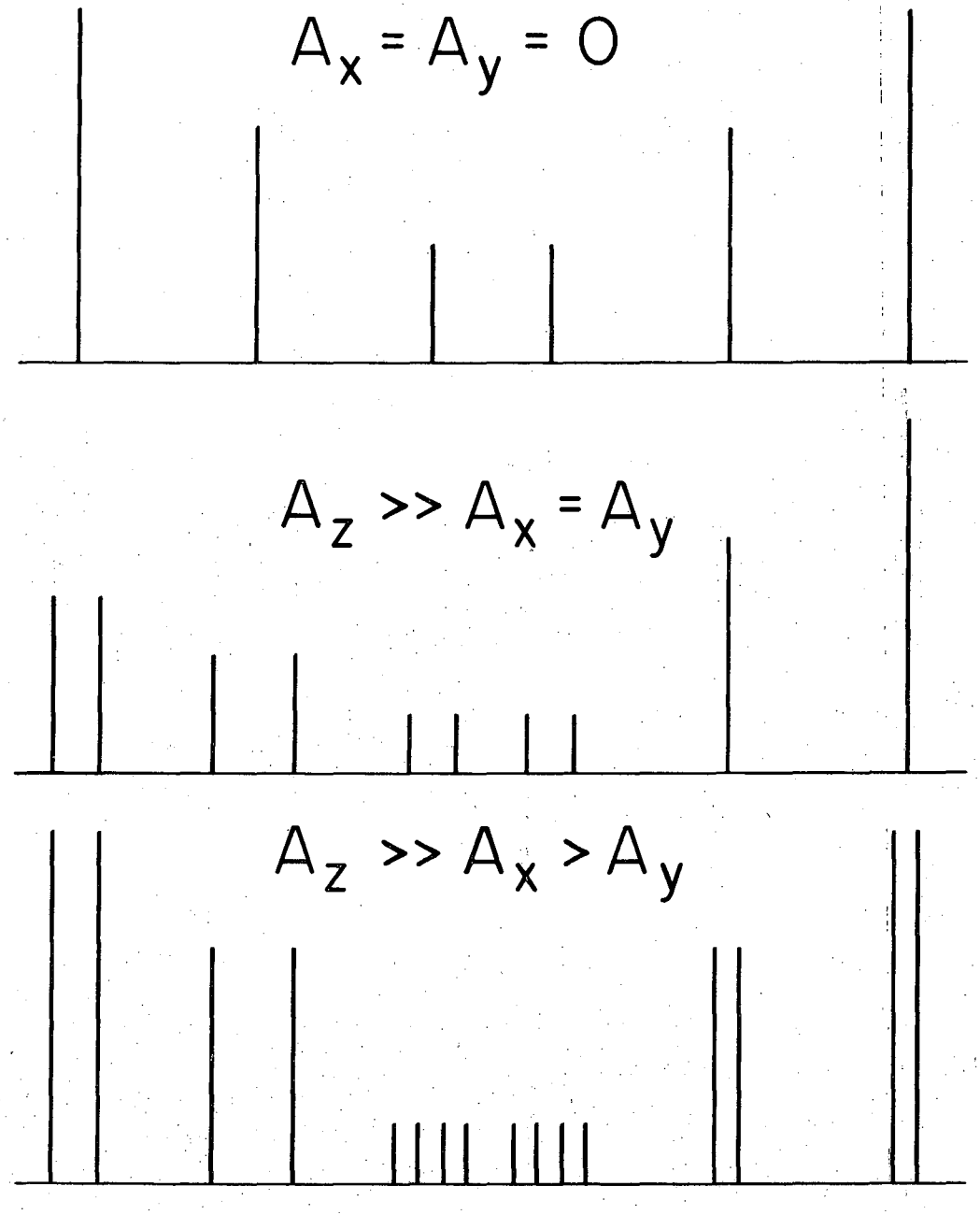


Fig. 6

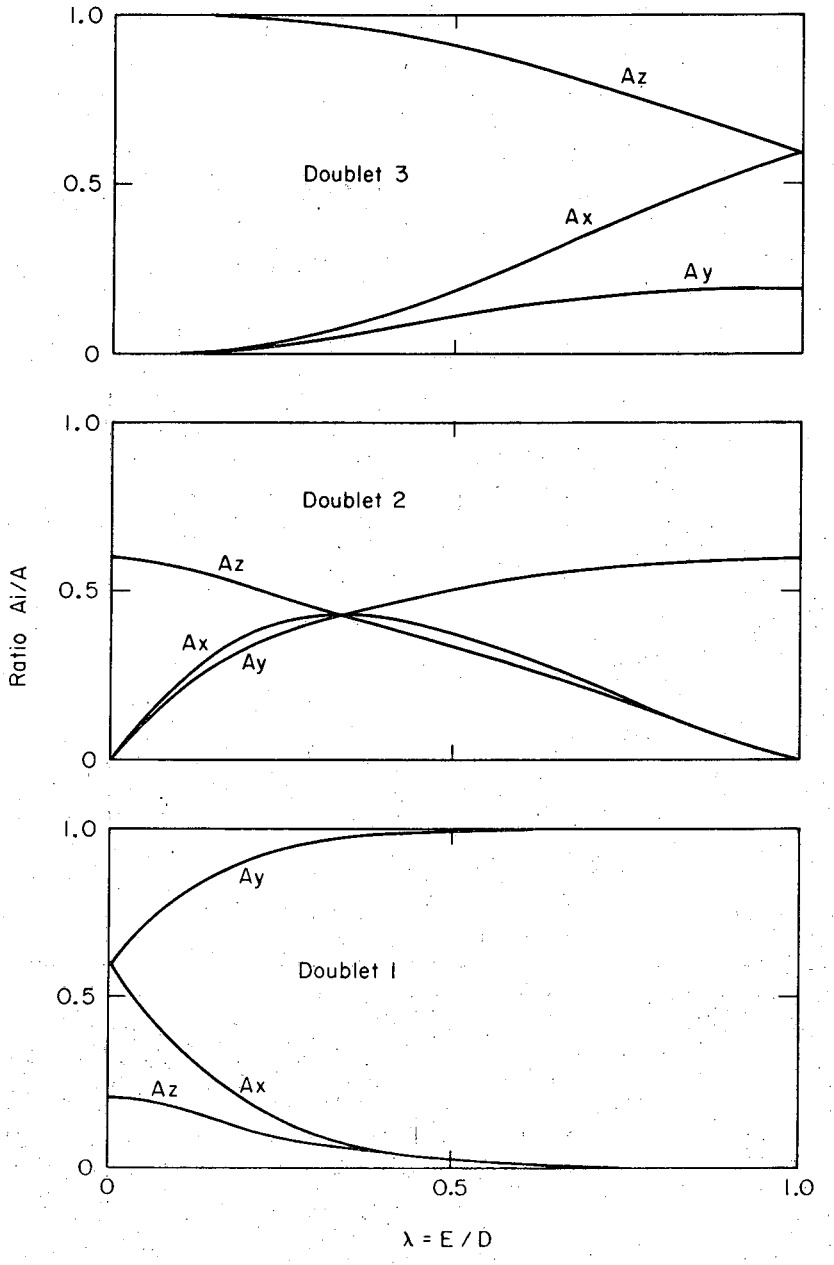
1.0
0.5
0
Az
Doublet 3
Ax
Ay
Doublet 2
Az
Ax
Ay
Ratio Ai/A
Doublet 1
Ay
Az
Ax
0
0.5
1.0
λ = E / D
MUB-9557

Fig. 7

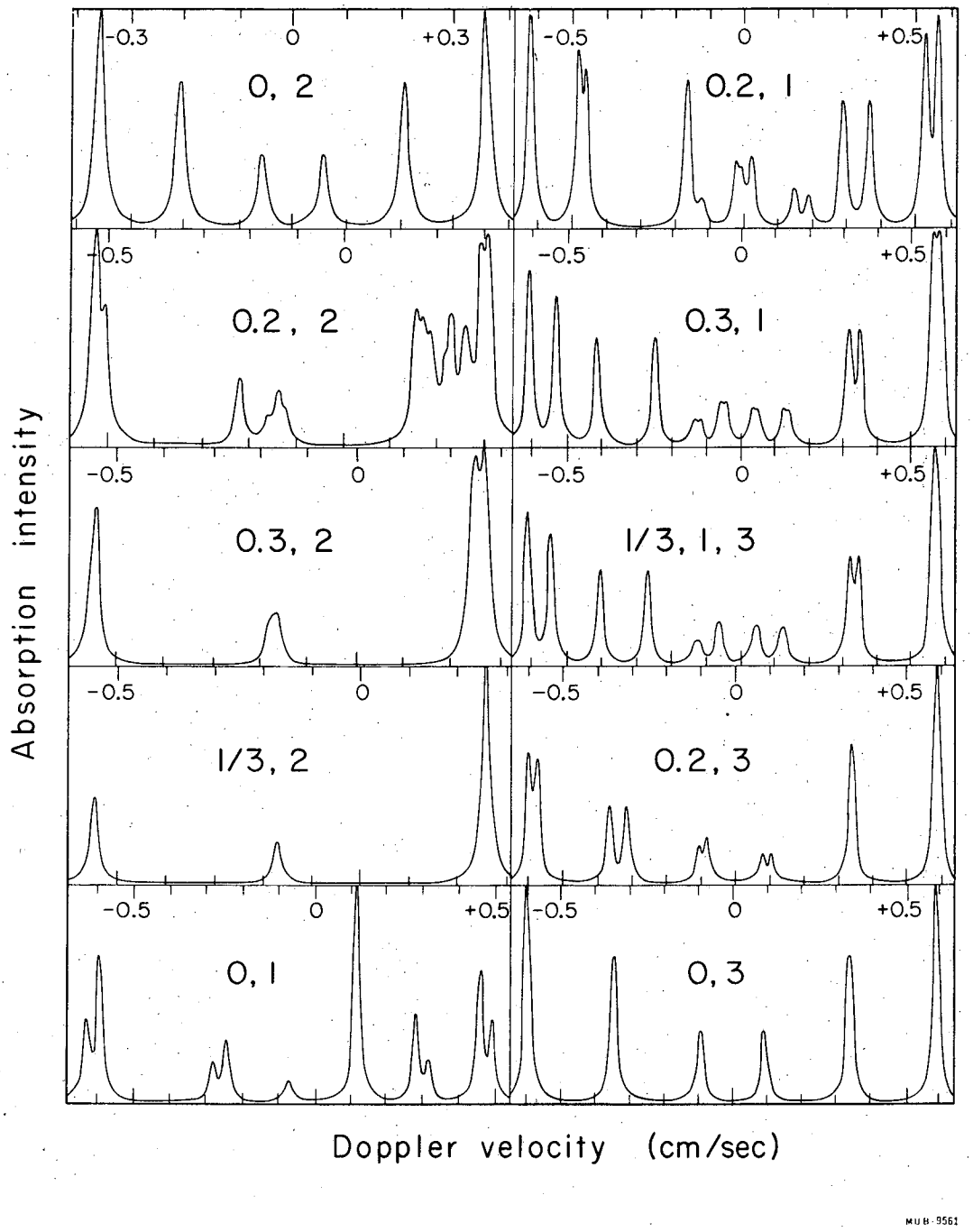
-0.3
0
+0.3
-0.5
0
+0.5
0, 2
0.2, 1
0.2, 2
0.3, 1
0.3, 2
1/3, 1, 3
1/3, 2
0.2, 3
0, 1
0, 3
Absorption intensity
Doppler velocity (cm/sec)
MUB-9561

Fig. 8

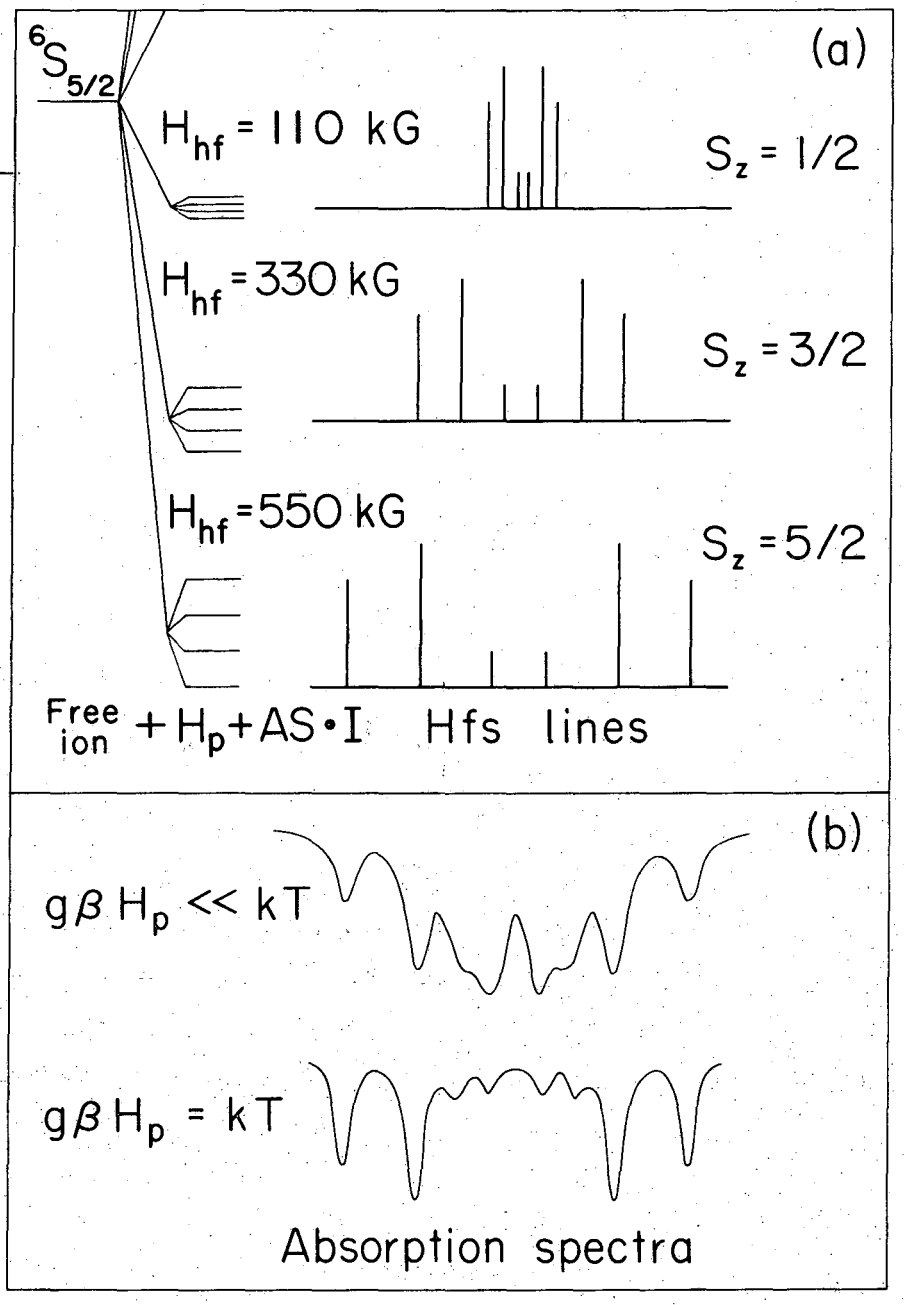
$^6S_{5/2}$
(a)
$H_{hf}$ = 110 kG
$S_z$ = 1/2
$H_{hf}$ = 330 kG
$S_z$ = 3/2
$H_{hf}$ = 550 kG
$S_z$ = 5/2
Free ion + $H_p$ + AS • I Hfs lines
(b)
$g\beta H_p \ll kT$
$g\beta H_p = kT$
Absorption spectra
MUB-9560

Fig. 9

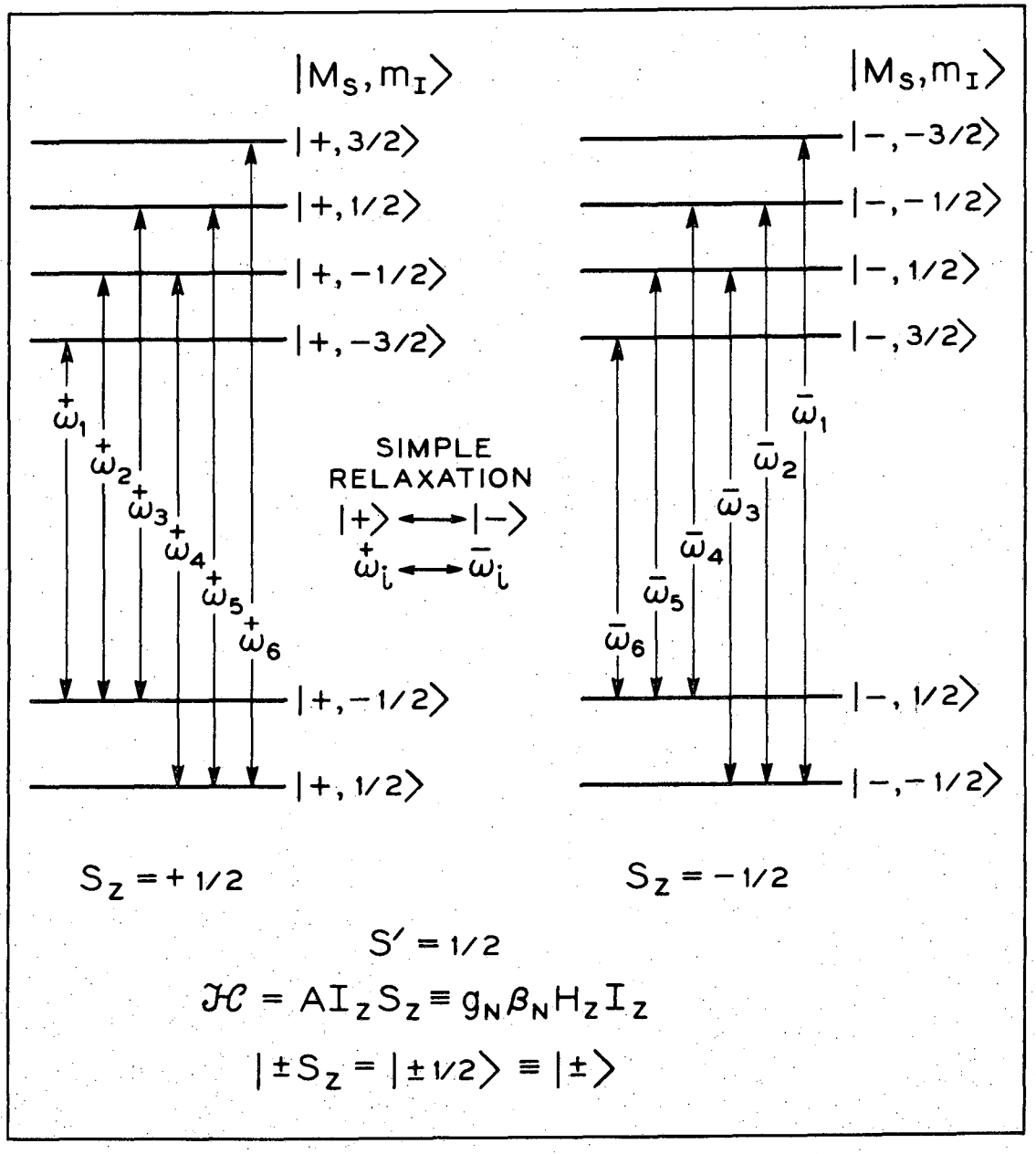


MUB-10295

Fig. 10

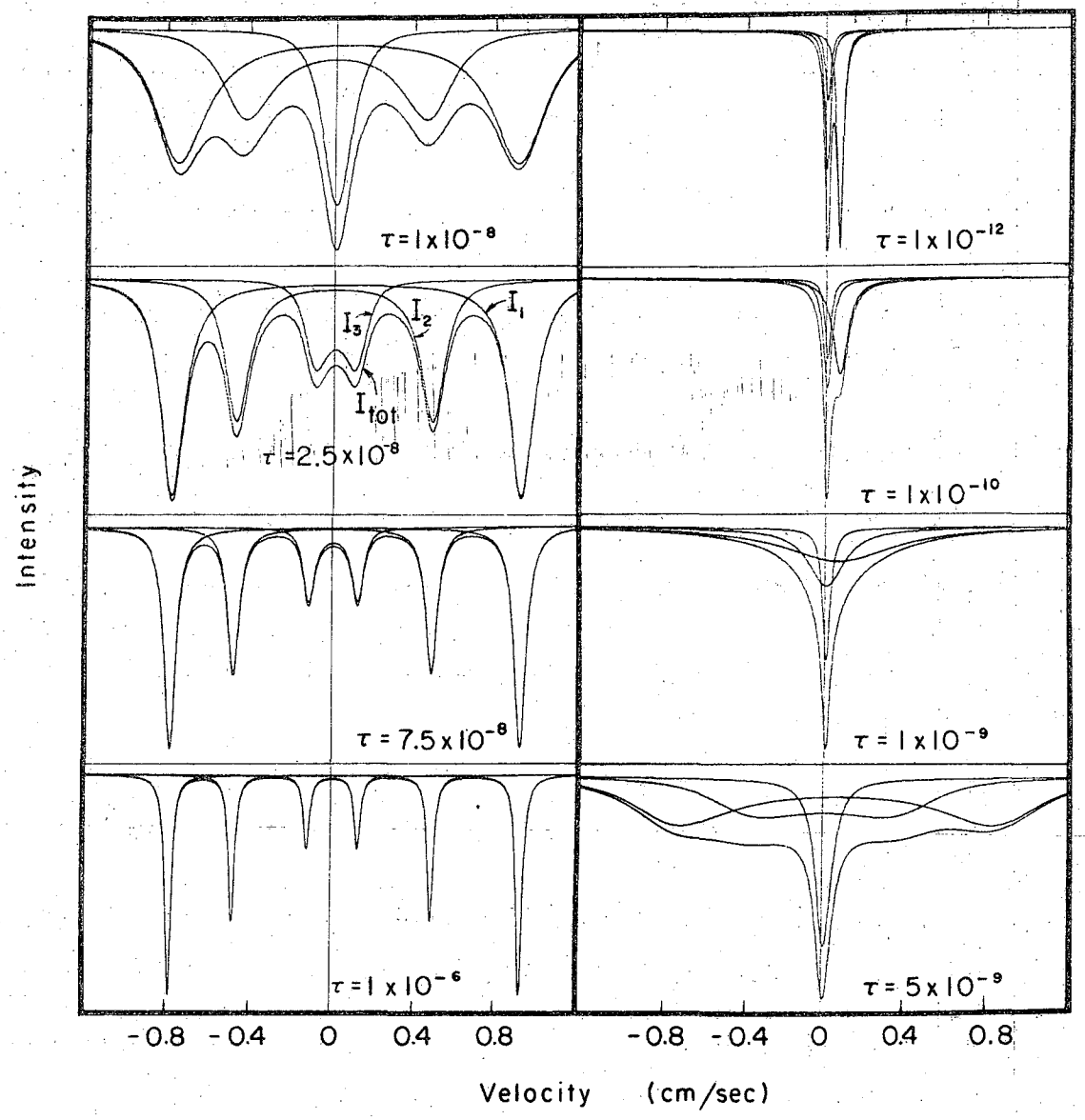
τ=1x10⁻⁸
τ=1x10⁻¹²
I₃
I₂
I₁
I_tot
τ=2.5x10⁻⁸
τ=1x10⁻¹⁰
τ=7.5x10⁻⁸
τ=1x10⁻⁹
τ=1x10⁻⁶
τ=5x10⁻⁹
Intensity
-0.8 -0.4 0 0.4 0.8
-0.8 -0.4 0 0.4 0.8
Velocity (cm/sec)
MUB-10710

Fig. 11